Controlled Oxygen Chemisorption on an Alumina Supported Rhodium Catalyst. Formation of a New Metal–Metal Oxide Interface Determined with Extended X-ray Absorption Fine Structure Spectroscopy

J. H. A. Martens, R. Prins,† and D. C. Koningsberger*

Eindhoven University of Technology, Laboratory of Inorganic Chemistry and Catalysis, P.O. Box 513, 5600 MB Eindhoven, The Netherlands *(Received: November 3, 1987; In Final Form: September 30, 1988)*

An alumina-supported rhodium catalyst has been studied with EXAFS. After reduction and evacuation, oxygen was admitted at 100 and 300 K. EXAFS spectra of the catalyst after oxygen admission at 100 K indicated the beginning of oxidation. At 300 K only a small part of the rhodium particles remained metallic and this metallic "kernel" was partly covered with rhodium oxide. In the rhodium metal to rhodium oxide interface the same 2.7-Å Rh^0–O^{2-} distances are present as in the metal–support interface. A model is presented that explains the observed formation of the rhodium metal–rhodium oxide interface.

Introduction

Oxidation of bulk metals is a process that is in general well understood.[1,2] In contrast, the oxidation of supported metal catalysts is less well understood. In technological applications, heterogeneous catalysts need to be regenerated several times and oxidation is an important step during the regeneration process of supported metal catalysts. Therefore, oxidation of small metal particles is a process that needs to be understood better. Two of the techniques that can be used to study the reduction and oxidation behavior of a catalyst are temperature programmed reduction (TPR) and temperature programmed oxidation (TPO).[3-10] Reduction of metal catalysts is in general a fast process and, hence, TPR is a very sensitive technique in describing the reducibility of supported metal catalysts.[3-6] Oxidation is in general a slow process, limited by diffusion of oxygen or metal ions through the oxidic skin around the metal particles, after the oxidation process has started.[1,2,7-10] Consequently, the usefulness of TPO is limited.

EXAFS is a technique that has proved to be very adequate in studying supported metal catalysts.[11,12] Here, we will present the results of an EXAFS study in which we followed the oxidation of small rhodium metal particles (25 ± 5 Å) at temeperatures of 100–300 K. In this temperature range, oxidation is not complete. A careful oxidation at room temperature is in general known as passivation.[7-10,13-16] As a result of the incompleteness of the oxidation, a cherrylike situation develops in which a small metallic kernel is covered with metal oxide.[16]

For highly dispersed supported metal catalysts, a careful analysis of the EXAFS spectra of the fully reduced sample usually indicates metal–oxygen distances to be present in the range of 2.6–2.8 Å.[12,17-23] These distances can be ascribed to OH^- neighbors of zerovalent metal atoms in the interface between metal particle and (hydroxylated) supporting oxide.[24]

Two observations confirm this assignment. The first is that these distances are always found when oxidic type supports are used (Al_2O_3,[12,17-20] TiO_2,[21,22] and even X zeolite[23]), and regardless of the metal (Rh,[12,17,21,22] Pt,[18] Ir,[19,20] Pd[23]), the distance is always in the range of 2.6–2.8 Å. Second, the relative number of O^{2-} neighbors decreases with increasing rhodium particle size,[12] indicating that these Rh–O distances are *not related to the bulk* of the metal particles but to the surface or the metal–support interface. In this study we will describe a detailed study of the beginning of the oxidation of small rhodium metal particles supported on γ-Al_2O_3. We will show that during oxidation new metal-to-metal oxide interfaces will be formed and that in these interfaces metal-to-oxygen distances are present in the range of 2.6–2.8 Å.

* To whom correspondence should be addressed.
† Present address: Technisch Chemisches Laboratorium, ETH Zentrum, CH-8092 Zürich, Switzerland.

Experimental Section

A 1.9 wt % Rh/Al_2O_3 catalyst was prepared by incipient wetting of the Al_2O_3 support (000-1.5E, Ketjen: 180 $m^2\ g^{-1}$, 0.65 mL g^{-1}) with an aqueous solution of $RhCl_3 \cdot 3H_2O$ (Drijfhout). After impregnation, the catalyst precursor was carefully dried (24 h at room temperature, 12 h at 395 K, heating rate 5 K min^{-1}). The dried catalyst was pressed into a thin self-supporting wafer with an absorbance (μx) of 2.5 at the rhodium K edge, assuring an optimum signal-to-noise ratio in the rhodium EXAFS spectra. The catalyst wafer was first reduced in an EXAFS in situ cell at 623 K (heating rate 5 K min^{-1}, 5 mL of H_2 min^{-1}), and after reduction, the catalyst was evacuated at the same temperature.

(1) Cabrera, N. *Semiconductor Surface Physics*; Kingston, R. H., Ed.; Wiley: New York, 1960.
(2) Hauffe, K. *The Surface Chemistry of Metals and Semiconductors*; Gatos, H. C., Ed.; Wiley: New York, 1960.
(3) Robertson, S. D.; McNicol, B. D.; de Baas, J. H.; Kloet, S. C.; Jenkins, J. W. *J. Catal.* **1975**, *37*, 424.
(4) Jenkins, J. W.; McNicol, B. D.; Robertson, S. D. *Chem. Tech.* **1975**, *7*, 316.
(5) Wagstaff, N.; Prins, R. *J. Catal.* **1979**, *59*, 435.
(6) Wagstaff, N.; Prins, R. *J. Catal.* **1979**, *59*, 445.
(7) Vis, J. C.; van 't Blik, H. F. J.; Huizinga, T.; van Grondelle, J.; Prins, R. *J. Catal.* **1985**, *95*, 333.
(8) van 't Blik, H. F. J.; Prins, R. *J. Catal.* **1986**, *97*, 188.
(9) Martens, J. H. A.; van 't Blik, H. F. J.; Prins, R. *J. Catal.* **1986**, *97*, 200.
(10) van 't Blik, H. F. J.; Koningsberger, D. C.; Prins, R. *J. Catal.* **1986**, *97*, 210.
(11) Sinfelt, J. H.; Via, G. H.; Lytle, F. W. *J. Chem. Phys.* **1977**, *67*, 3831.
(12) van Zon, J. B. A. D.; Koningsberger, D. C.; van 't Blik, H. F. J.; Sayers, D. E. *J. Chem. Phys.* **1985**, *12*, 5742.
(13) Uchijima, T.; Herrmann, J. M.; Inoue, Y.; Burwell, R. L., Jr.; Butt, J. B.; Cohen, J. B. *J. Catal.* **1977**, *50*, 464.
(14) Koboyashi, M.; Inoue, Y.; Takahashi, N.; Burwell, R. L., Jr.; Butt, J. B.; Cohen, J. B. *J. Catal.* **1980**, *64*, 74.
(15) Nandi, R. K.; Georgopoulos, P.; Cohen, J. B.; Butt, J. B.; Burwell, R. L., Jr. *J. Catal.* **1982**, *77*, 421.
(16) Huizinga, T.; van Grondelle, J.; Prins, R. *Appl. Catal.* **1984**, *10*, 199.
(17) Koningsberger, D. C.; van Zon, J. B. A. D.; van 't Blik, H. F. J.; Mansour, A. N.; Visser, G. J.; Prins, R.; Sayers, D. E.; Short, D. R.; Katzer, J. R. *J. Phys. Chem.* **1985**, *89*, 4075.
(18) Koningsberger, D. C.; Sayers, D. E. *Solid State Ionics* **1985**, *16*, 23.
(19) van Zon, F. B. M.; Visser, G. J.; Koningsberger, D. C. *Proceedings 9th International Congress on Catalysis, Calgary*; Phillips, M. J., Ternan, M., Eds.; The Chemical Institute of Canada: Ottawa, 1988; Vol. 3, p 1386.
(20) Duivenvoorden, F. B. M.; Koningsberger, D. C., to be submitted for publication.
(21) Koningsberger, D. C.; Martens, J. H. A.; Prins, R.; Short, D. R.; Sayers, D. E. *J. Phys. Chem.* **1986**, *90*, 3047.
(22) Martens, J. H. A.; Prins, R.; Zandbergen, H.; Koningsberger, D. C. *J. Phys. Chem.* **1988**, *92*, 1903.
(23) Moller, K.; Bein, T. *EXAFS and Near Edge Structure*; Lagarde, P., Raoux, D., Petiau, J., Eds.; Les Editions de Physique: Les Ulis, France, 1986; Vol. 1, pp C8-231.
(24) Martens, J. H. A.; Thesis, Eindhoven University of Technology, The Netherlands, 1988.

0022-3654/89/2093-3179$01.50/0

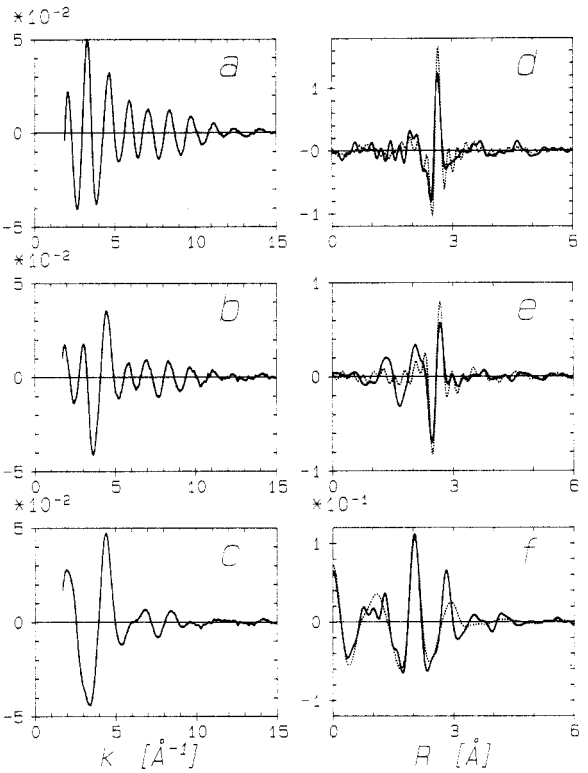

Figure 1. Raw EXAFS data of (a) Rh/Al_2O_3 after reduction and evacuation at 623 K; (b) Rh/Al_2O_3 after oxygen exposure at 100 K; (c) Rh/Al_2O_3 after oxygen admission at 300 K. Imaginary parts of the Fourier transforms of the original EXAFS spectra in panels a–b (solid lines) and calculated Rh–Rh EXAFS spectra (dashed lines). The Fourier transforms are k^1-weighted and corrected for the Rh–Rh phase shift and backscattering amplitude. The Fourier transform ranges in k-space are indicated in parentheses. (d) Rh/Al_2O_3 after reduction and evacuation at 623 K (2.97–14.58); (e) Rh/Al_2O_3 after oxygen exposure at 100 K (3.26–12.03). (f) Imaginary part of Fourier transform (k^1-weighted, corrected for Rh–O phase shift, Δk = 2.55–12.45) of EXAFS spectrum of Rh/Al_2O_3 after oxygen admission at 300 K (solid line) and calculated dominant Rh^{3+}–O^{2-} contribution.

After this, an EXAFS spectrum was recorded with the sample at 100 K. Then oxygen (0.1 atm partial pressure) was admitted at the same temperature, and after 10 min a second EXAFS spectrum was recorded. Thereafter, the sample was allowed to warm to 300 K under oxygen, and after 10 min at 300 K, the catalyst was quickly cooled down to 100 K and a third EXAFS spectrum was recorded. The EXAFS spectra were recorded at the synchrotron radiation source (SRS) in Daresbury, U.K. The storage ring was operated at 2.0 GeV; the ring current was in the range of 100–300 mA.

In order to analyze the EXAFS spectra of the catalyst, EXAFS spectra of reference compounds are needed. From these, backscattering amplitude ($F(k)$) and phase shift ($\phi/(k)$) functions have to be extracted. With these functions, we can calculate EXAFS spectra for the catalyst samples. In the calculations we have four independent parameters, the coordination number N, the coordination distance R, the Debye–Waller factor $\Delta\sigma^2$, which accounts for disorder, and E_0, which allows for a correction on the position of the adsorption edge. By changing these parameters, EXAFS spectra that fit the measured spectra best are calculated. Rhodium foil was used as a reference for the Rh^0–Rh^0 contributions and Rh_2O_3 as a reference for Rh^0–O^{2-} and Rh^{3+}–O^{2-} contributions. The thickness of the rhodium foil was 20 μm (corresponding to an absorbance μx = 1.4). For Rh_2O_3 a wafer with an absorbance of 2.5 was prepared by mixing and crushing 70 mg of Rh_2O_3 with 30 mg of Al_2O_3. The EXAFS spectra of the reference compounds were recorded with the sample at room temperature.

Data Analysis and Results

The EXAFS functions, $\chi(k)$, were obtained from the X-ray absorption spectra by subtracting a Victoreen curve, followed by a cubic spline background removal.[25] Normalization was performed by division to the height of the edge. In Figure 1a–c, the raw EXAFS spectra of the catalyst after reduction and evacuation, after oxygen admission at 100 K, and after warming to 300 K are shown.

For a complete description of the analysis procedure we refer to ref 12, 22, 26, and 27. Briefly, the analysis consisted of the following steps which led to a recurrent optimization process. For the reduced and evacuated sample and for the sample oxidized at 100 K, an Rh–Rh EXAFS function was calculated with $F(k)$ and $\phi(k)$ obtained from rhodium foil. The parameters N, R, $\Delta\sigma^2$, and E_0 were optimized to give the best agreement in r-space of the main peaks in a k^3-weighted Fourier transform. In Figure 1d,e the k^1-weighted Fourier transforms of the experimental data and the calculated Rh–Rh EXAFS functions are shown. Corrections were made in the Fourier transformation for the k dependence in backscattering amplitude and phase shift using $F(k)$ and $\phi(k)$ of the rhodium foil.[17] From Figure 1d,e it is obvious that, apart from a Rh–Rh contribution, other contributions are present. Note that these differences are less obvious in a k^3-weighted Fourier transform. The calculated Rh–Rh EXAFS spectrum was subtracted from the measured spectrum. The resulting difference spectrum contained two Rh–O contributions. A two-shell Rh–O EXAFS function (using $F(k)$ and $\phi(k)$ from Rh_2O_3) and its Fourier transform were calculated to give the best agreement with the difference spectrum and with the k^1-weighted Fourier transform of the difference spectrum (corrected for the k dependence in the Rh–O phase shift). In Figures 2a,b the k^1-weighted Rh–O corrected Fourier transforms of the difference spectra and the calculated two-shell Rh–O spectra are shown. This calculated two-shell Rh–O EXAFS function was again subtracted from the experimental data, in order to obtain a difference spectrum with a major Rh–Rh contribution and almost no Rh–O contributions. Again a best fitting Rh–Rh EXAFS function was calculated, subtracted from the experimental data in order to once more optimize the Rh–O contributions. In Figure 2d,e the k^1-weighted Rh–Rh corrected Fourier transforms of the experimental data and the Fourier transforms of the sum of the calculated Rh–Rh and two-shell Rh–O EXAFS functions are shown. The results of this analysis procedure are presented in Table I.

For the sample that has been oxidized at 300 K, the procedure was different. Because in this case the main contribution originated from oxygen neighbors, a Rh^{n+}–O^{2-} EXAFS spectrum using $F(k)$ and $\phi(k)$ from Rh_2O_3 was calculated first to give the best agreement in the k^1-weighted Rh–O corrected Fourier transform with the experimental data. Figure 1f shows the k^1-weighted Rh–O corrected Fourier transform of the experimental data and the calculated Rh^{n+}–O^{2-} EXAFS function. The re-

TABLE I: Final Results from EXAFS Data Analysis[a]

treatment	NN	coord no.[b]	distance,[b] Å	$\Delta\sigma^2$,[b,c] $\times 10^{-3}$ Å^2	E_0,[b,c] eV
R623–E623	Rh	5.6 (0.2)	2.635 (0.005)	3 (1)	1.7 (1)
	O	0.6 (0.3)	2.055 (0.01)	1 (2)	8.4 (2)
	O	2.0 (0.2)	2.73 (0.01)	2.5 (1)	−4.1 (2)
R623–E623–O100	Rh	4.1 (0.2)	2.63 (0.005)	3.4 (1)	7.9 (1)
	O	1.4 (0.2)	2.055 (0.01)	1 (2)	−2.5 (1)
	O	1.4 (0.2)	2.77 (0.05)	2.5 (1)	−2.9 (1)
R623–E623–O100–O300	Rh	1.9 (0.3)	2.645 (0.01)	4.4 (2)	4 (2)
	O	3.6 (0.3)	2.03 (0.01)	4.7 (2)	−0.5 (2)
	O	1.7 (0.3)	2.76 (0.03)	6 (3)	4 (2)

[a] NN, nearest neighbor. R, reduction in H_2 at the temperature indicated; E, evacuation at the temperature indicated; O, admission of oxygen at the temperature indicated. [b] Estimated overall (experimental + systematic) error is given in parentheses. [c] $\Delta\sigma^2$, the Debye–Waller factor, is a measure for the disorder and E_0 is a correction on the edge position; see ref 12 for more details.

(25) Cook, J. W.; Sayers, D. E. *J. Appl. Phys.* **1981**, *52*, 5024.
(26) Duivenvoorden, F. B. M.; Koningsberger, D. C.; Uh, Y. S.; Gates, B. C. *J. Am. Chem. Soc.* **1986**, *108*, 6254.
(27) van 't Blik, H. F. J.; van Zon, J. B. A. D.; Huizinga, T.; Vis, J. C.; Koningsberger, D. C.; Prins, R. *J. Am. Chem. Soc.* **1985**, *107*, 3139.

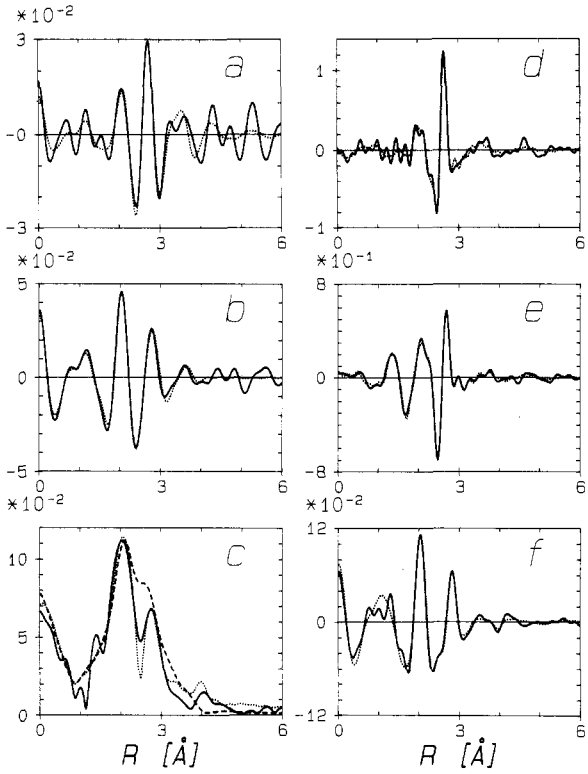

Figure 2. Imaginary parts of the Fourier transforms of the difference spectra (original EXAFS spectra minus the calculated Rh–Rh EXAFS functions (solid lines) and the Fourier transforms of the calculated two-shell Rh–O EXAFS functions (dashed lines). The Fourier transforms are k^1-weighted and corrected for Rh–O phase shift. The Fourier transform ranges in k-space are indicated in brackets. (a) Rh/Al_2O_3 after reduction and evacuation at 623 K (3.46–8.33). (b) Rh/Al_2O_3 after oxygen exposure at 100 K (2.54–8.00). (c) Magnitude of the Fourier transform of: solid line, Rh/Al_2O_3 after oxygen admission at 300 K (2.55–12.45); dotted line, calculated Rh^{3+}–O^{2-} + Rh^0–Rh^0 EXAFS function; dashed line, calculated Rh^{3+}–O^{2-} + Rh^0–O^{2-} EXAFS function. (See text for further details.) Fourier transform of the original EXAFS spectra (solid lines) and the Fourier transforms of the calculated best fitting EXAFS spectra using the parameters presented in Table I. The Fourier transforms are k^1-weighted, d and e are corrected for Rh–Rh phase shift and backscattering amplitude, and f is corrected for the Rh–O phase shift. The Fourier transform ranges in k-space are indicated in parentheses. (d) Rh/Al_2O_3 after reduction and evacuation at 623 K (2.97–14.58). (e) Rh/Al_2O_3 after oxygen exposure at 100 K (3.26–12.03). (f) Rh/Al_2O_3 after oxygen admission at 300 K (2.55–12.45).

maining difference spectrum could be fitted with a combination of two contributions, a Rh^0–Rh^0 and a Rh^0–O^{2-} EXAFS function. The major contribution in the difference spectrum originates from oxygen scatterers. Therefore, a k^1-weighted Rh–O phase-corrected Fourier transform rather than a k^3-weighted Fourier transform (corrected for Rh–Rh phase and backscattering amplitude) was used to optimize the different contributions in the EXAFS spectrum. Since in this Fourier transform an incorrect phase shift function is used for the (small) Rh^0–Rh^0 contribution, the accompanying Rh–Rh peak is shifted and coincides with the peak originating from the Rh^0–O^{2-} bond of about 2.76 Å. The fact that the peak at the right-hand side of the Rh^{3+}–O^{2-} contribution in Figure 1f is indeed the result of two contributions (Rh^0–Rh^0 and Rh^0–O^{2-}) becomes clear from a careful study of Figure 2c. In Figure 2c, the magnitude of the Fourier transform of the original data (solid line) and of the Fourier transforms of a calculated Rh^{3+}–O^{2-} + Rh^0–Rh^0 EXAFS spectrum (dotted line) and of a calculated Rh^{3+}–O^{2-} + Rh^0–O^{2-} EXAFS spectrum (dashed line) are presented. In the Fourier transform of the former calculated EXAFS function, a strong destructive interference is visible in the region between both peaks, whereas in the latter a slightly constructive interference is observed. In the same region in the Fourier transform of the original data, a slightly destructive interference is present. Therefore, we conclude that the right-hand side peak in Figure 2c is the result of the sum of two contributions, namely, Rh^0–Rh^0 and Rh^0–O^{2-}. In a k^1-weighted Rh–Rh phase and backscattering amplitude corrected Fourier transform, all contributions are separated, but as mentioned above, this Fourier transform is not suitable to optimize the dominant low-Z scatterer contribution. Figure 2f shows once again the k^1-weighted Rh–O corrected Fourier transforms of the experimental data and the calculated (Rh^{n+}–O^{2-} + Rh^0–O^{2-} + Rh^0–Rh^0) EXAFS functions. The results of this analysis are also presented in Table I. Because of the more difficult data analysis of the sample oxidized at 300 K, the uncertainties of the final EXAFS parameters of this sample are larger than those of the other samples.

Even though the EXAFS spectra of the catalyst were measured at 100 K and those of the reference compounds at room temperature, all resulting $\Delta\sigma^2$ values were positive, indicating that some degree of disorder is present in the catalyst. The results are in full agreement with former EXAFS data of fully reduced Rh/Al_2O_3 measured at 100 and 300 K.[12]

Discussion

1. Rh/Al_2O_3 after Reduction and Evacuation. After reduction and evacuation of the catalyst at 623 K the major contribution in the EXAFS spectrum is from rhodium neighbors. In the difference spectrum (see Figure 2a) two contributions are present that both originate from oxygen neighbors.

The rhodium atoms and ions in the sample have on the average 5.6 rhodium nearest neighbors. The coordination distance of 2.635 Å points to zerovalent rhodium atoms having zerovalent rhodium neighbors; the contribution originates from rhodium atoms in metallic particles. From ref 28 we can estimate that the particles contain about 15 atoms on the average and are roughly 10 Å in diameter. However, the results underestimate the size of the metal particles. For, in the EXAFS spectrum, an additional contribution from oxygen neighbors at 2.055 Å is present and this contribution arises from oxidic type Rh^{n+}–O^{2-} bonds. From TPR studies, which are usually carried out in 5% H_2 in some inert gas, it is evident that at 623 K reduction in 100% H_2 should have been complete.[12] During the evacuation procedure at high temperature, however, the hydroxylated Al_2O_3 surface loses water and at the high evacuation temperature, the metal particles may possibly be partly reoxidized by H_2O. Another possibility is that a small leakage of air into the cell has occurred during the evacuation procedure. Anyway, it is obvious that the metal particles were partly oxidized after the reduction treatment, during the evacuation procedure. In bulk Rh_2O_3 the Rh^{3+}–O^{2-} distance is 2.05 Å and each rhodium ion has six oxygen neighbors. We found a Rh^{n+}–O^{2-} coordination number of 0.6. The coordination numbers measured with EXAFS are averaged coordination numbers, i.e., they are averaged over all rhodium atoms and ions present in the sample. The zerovalent rhodium atoms in the metal particles will not have oxygen neighbors at an oxidic type distance. The rhodium ions in an oxidic phase in the catalyst will have only oxygen neighbors in their first coordination shell at about 2.05 Å. If we assume that the rhodium ions in the oxidic phase in the catalyst have four to six oxygen neighbors, this means that 15–10% of the rhodium atoms are oxidized ($0.6/4 = 0.15 > f_{ox} > 0.6/6 = 0.10$; f_{ox} is the fraction of rhodium atoms that have been oxidized). Because the Rh–Rh coordination number of 5.6 is also an average coordination number, the Rh–Rh coordination number of rhodium atoms present in metallic particles must be corrected as follows: $N_{corr} = N_{meas}/f_{red}$ in which $f_{red} = 1 - f_{ox} = 0.85$–$0.90$. As a consequence, the average Rh–Rh coordination number is 6.4 ± 0.2 and the metal particles will consist approximately of 25 atoms; their diameter is about 15 Å. Also, although the catalyst had been reduced at high temperature (623 K), after evacuation the sample was partly oxidized, as can be concluded from the presence of the Rh^{n+}–O^{2-} distance of 2.05 Å.

One more contribution needs to be discussed—the 2.73 Å Rh–O contribution (cf. Table I). This contribution arises from oxygen

(28) Kip, B. J.; Duivenvoorden, F. B. M.; Koningsberger, D. C.; Prins, R. *J. Catal.* **1987**, *105*, 26.

ions in the surface of the support, which are neighbors to zerovalent rhodium atoms in the metal–support interface. This type of rhodium-to-oxygen contribution has frequently been reported.[12,17-23] Like the Rh–Rh contribution, this Rh^0–O^{2-} contribution must be corrected for the presence of rhodium oxide. The corrected coordination number is $2.0/(1 - f_{ox}) = 2.3 \pm 0.1$. However, this number does not yet represent the number of oxygen anions in contact with rhodium atoms *in the metal–support interface*, because for three-dimensional particles only part of the rhodium atoms will be present in this interace. To be able to deduce the real number of neighboring oxygen ions for a rhodium atom in the metal–support interface we need to know the size *and* the shape of the metal particles. The size is obtained from the Rh–Rh coordination number, but no information on the shape is available. Alternatively, if we know the real number of oxygen neighbors for an interfacial rhodium metal atom, we can determine the shape of the metal particles. In the following we assumed that the rhodium metal particles rest on a hydroxylated [111] face of the γ-Al_2O_3 support. The size of the rhodium atoms is about equal to and size of the oxygen ions (the Rh–Rh distance is 2.635 Å; the O^{2-}–O^{2-} distance is 2.80 Å), and the real Rh^0–O^{2-} coordination number of a rhodium atom in the metal support interface is 3.0. With this knowledge we can make a model for the size and shape of the metal particles.

2. *A Model for the Oxidation of Metal Particles.* In this paper we will try to describe the oxidation process of small metal particles. At low temperatures, oxygen readily adsorbs and even partially dissociates on rhodium metal.[29] Considering the fact that we study very small metal particles, oxidation may be a relatively fast process. In the following, we will assume that the metal atoms in the particle with the least negative binding energy (i.e., atoms that are the most coordinatively unsaturated) will be oxidized first. We have calculated the cohesive energy of every atom in the metal particle by summation of the Lennard-Jones energy contributions of all the other atoms in the metal particle. We assumed that this cohesive energy was not affected by the shape of the metal particle, its size, etc. In addition we neglected the contribution of neighboring oxygen ions and consequently the influence of the orientation of the metal particle on the support. Altogether these assumptions make that this model is only a first approximation for the cohesive energy in these small metal particles. In comparison with only counting the number of nearest neighbors, this model introduces a kind of long-range ordering effect, and we expect that it is therefore more accurate. The Lennard-Jones binding energy is given by

$$E(R) = A\left(\frac{1}{R^{12}} - \frac{B}{R^6}\right)$$

where R is the interatomic rhodium–rhodium distance. The constant A in the expression is not important when one compares binding energies of the same type and has therefore been taken equal to unity. B determines the interatomic distance at which the minimum in the binding energy occurs and has been given the value of 0.005 989 Å^6. This value corresponds to $R_{min} = 2.635$ Å, which is equal to the Rh–Rh distance in the metal particles (see Table I). Thus, the relative binding energy of atom i in the metal particle has been calculated by using

$$E = \sum_{i \neq j}\left[\frac{1}{R_{ij}^{12}} - \frac{5.989 \times 10^{-3}}{R_{ij}^{6}}\right]$$

In most cases, the R_{ij}^{-12} term is negligible compared to the R_{ij}^{-6} term. Therefore, a model in which only the number of nearest rhodium neighbors is taken as a measure for the binding energy of a given atom gives nearly the same result as the model described above, which takes into account the long-range interactions as well. In Table II are presented the calculated binding energies and the number of rhodium nearest neighbors during a hypothetical oxidation process in which the rhodium atoms, one by one, become "oxidized" to Rh^{n+}. Once a rhodium atom is oxidized, it will preferentially be surrounded by O^{2-} ions. Hence, it will not contribute to the EXAFS Rh^0–Rh^0 coordination number and it will also not contribute to the binding energy of the remaining rhodium atoms in the metal particle. After an atom has been oxidized (i.e., removed from the actual cluster), the new Rh^0–Rh^0

(29) Matsushima, T. *Surf. Sci.* **1985**, *157*, 297.

TABLE II: Lennard-Jones Binding Energies and Number of Rhodium Neighbors for Each Rhodium Metal Atom during a Hypothetical Oxidation Process[a]

atom no.		number of atoms oxidized									
		0	1	2	3	4	5	6	7	8	9
1	$-E$	4.1	3.2								
	N	4	3								
2, 3	$-E$	6.0	5.9	5.0	5.0	5.0	5.0	5.0	5.0	5.0	5.0
	N	6	6	5	5	5	5	5	5	5	5
4	$-E$	4.1	4.1	4.0	3.2						
	N	4	4	4							
5	$-E$	4.0									
	N	4									
6	$-E$	8.7	7.8	6.9	6.9	6.9	6.9	6.9	6.8	6.0	5.9
	N	9	8	7	7	7	7	7	7	6	6
7	$-E$	9.1	9.1	9.0	9.0	9.0	8.9	8.9	8.8	8.8	8.7
	N	9	9	9	9	9	9	9	9	9	9
8	$-E$	8.7	8.7	8.7	7.8	6.9	6.9	6.9	6.8	6.8	6.0
	N	9	9	9	8	7	7	7	7	7	6
9	$-E$	4.0	4.0	4.0							
	N	4	4	4							
10, 13	$-E$	5.9	5.0	4.9	4.9	4.9	4.0	4.0	4.0		
	N	6	5	5	5	5	4	4	4		
11, 12	$-E$	8.8	8.8	8.7	8.8	8.7	7.9	7.8	6.9	6.0	6.0
	N	9	9	9	9	9	8	8	7	6	6
14	$-E$	4.1	4.1	4.1	4.1	4.1					
	N	4	4	4	4	4					
15	$-E$	5.2	5.2	5.2	5.2	5.2	4.3	3.4			
	N	5	5	5	5	5	4	3			
16	$-E$	4.1	4.1	4.1	4.1	4.1	4.0				
	N	4	4	4	4	4	4				
17	$-E$	6.1	5.9	5.0	5.0	5.0	5.0	5.0	5.0	4.9	4.9
	N	6	6	5	5	5	5	5	5	5	5
18	$-E$	7.1	7.1	7.0	7.0	6.9	6.9	6.9	6.9	6.9	6.9
	N	7	7	7	7	7	7	7	7	7	7
19	$-E$	6.1	6.1	6.1	5.9	5.0	5.0	5.0	5.0	5.0	4.9
	N	6	6	6	6	5	5	5	5	5	5
20	$-E$	6.0	5.2	5.0	5.0	5.0	4.9	4.9	4.9	4.0	4.0
	N	6	5	5	5	5	5	5	5	4	4
21, 22	$-E$	9.0	9.0	8.9	8.9	8.9	8.8	8.8	8.8	8.6	8.6
	N	9	9	9	9	9	9	9	9	9	9
23	$-E$	6.0	6.0	6.0	5.2	5.0	5.0	4.9	4.9	4.9	4.0
	N	6	6	6	5	5	5	5	5	5	4
24, 26	$-E$	6.1	6.0	6.0	6.0	6.0	5.1	5.1	4.9	4.0	4.0
	N	6	6	6	6	6	5	5	5	4	4
25	$-E$	7.2	7.2	7.2	7.2	7.2	7.0	6.8	6.0	5.9	5.8
	N	7	7	7	7	7	7	7	6	6	6

[a] E, Lennard-Jones binding energy in arbitrary units (see text); N, number of rhodium nearest neighbors.

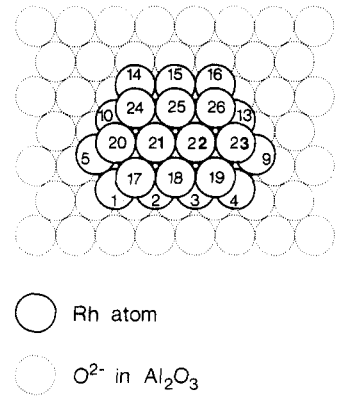

Figure 3. Twenty-six atom rhodium metal particle (fcc structured) on a [111] γ-Al_2O_3 surface.

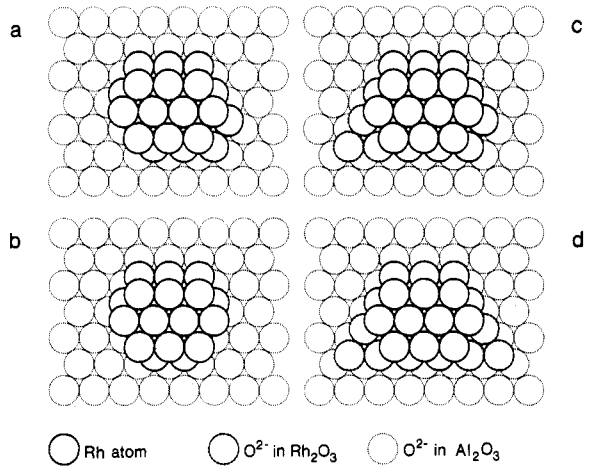

Figure 4. Model of the rhodium metal particles of γ-Al_2O_3 after evacuation: (a) bare 24-atom rhodium metal particle; (b) bare 22-atom rhodium metal particle; (c) 24-atom rhodium metal particle in contact with Rh_2O_3; (d) 22-atom rhodium metal particle in contact with Rh_2O_3.

coordination number, the binding energy, and the number of rhodium neighbors for each rhodium atom in the remaining particle were recalculated.

In Figure 3, a 26-atom metal particle resting on a [111] γ-Al_2O_3 face is drawn. The averaged Rh–Rh coordination number is 6.38. The particle is assumed to be grown epitaxially on an alumina [111] crystal face, which according to ref 30 is the most stable crystal face. In the 26-atom metal particle in Figure 3, atom number 5 and atom number 9 have the lowest binding energy. The atoms with the next lowest binding energy are atoms 1 and 4. With f_{ox} = 0.10–0.15, it follows that about three rhodium atoms in this particle were oxidized. Removing (arbitrarily) atom 5 from the particle induces a new situation in which atom 1 has the lowest binding energy in the 25-atom metal particle (see Table II, column under 1). After subsequently removing atom 1, atom 9 has (again) the lowest binding energy. When atom 9 is removed as well, the Rh–Rh coordination number averaged over all 23 atoms and 3 ions equals 5.54 (i.e., the coordination number as it would have been measured with EXAFS), in excellent agreement with the experimentally observed value of 5.6. However, after removing atom 9, atom 4 obtains a very low binding energy (Table II, column under 3). We therefore assume that when atom 9 is oxidized, atom number 4 will immediately be oxidized as well. As a consequence, the situation after reduction and evacuation will be represented by an average of two situations, one in which two atoms (atoms 1 and 5 or 9 and 4) and one in which four atoms (atoms 1, 5, 9, and 4) are oxidized. The situation in which three atoms are oxidized is unlikely to occur. In Figure 4a,b, a bare 24- and 22-atom metal particles are shown. For these metal particles, the calculated Rh^0–O^{2-} coordination number is on the average equal to 1.5 (1.38 and 1.62 respectively; note that these are already average coordination numbers), which is too low compared to the measured value of 2.0. However, up to now we have only considered O^{2-} anions of the support which are in contact with the remaining metallic rhodium atoms. But the rhodium oxide phase which has been formed may well be in contact with the remaining metal particle, and this would explain the higher Rh^0–O^{2-} coordination number. In Figure 4c,d, a possibility is presented in which several oxygen ions take the place of the oxidized rhodium atoms. Using that configuration, the calculated and averaged Rh^0–O^{2-} coordination number is 2.0. We have assumed that the oxidation process leads to stoichiometric Rh_2O_3 and thus, in Figure 4 (as well as in Figures 5 and 6) three O^{2-} ions are incorporated for every two rhodium atoms that are assumed to be oxidized to Rh^{3+}. The Rh^{3+} ions are not shown in these figures. They most probably reside in the octahedral or tetrahedral sites present between the oxygen ions from the support and the oxygen ions in the rhodium oxide phase.

(30) Knözinger, H.; Ratnasamy, P. *Catal. Rev. Sci. Eng.* **1978**, *17*(1), 31.

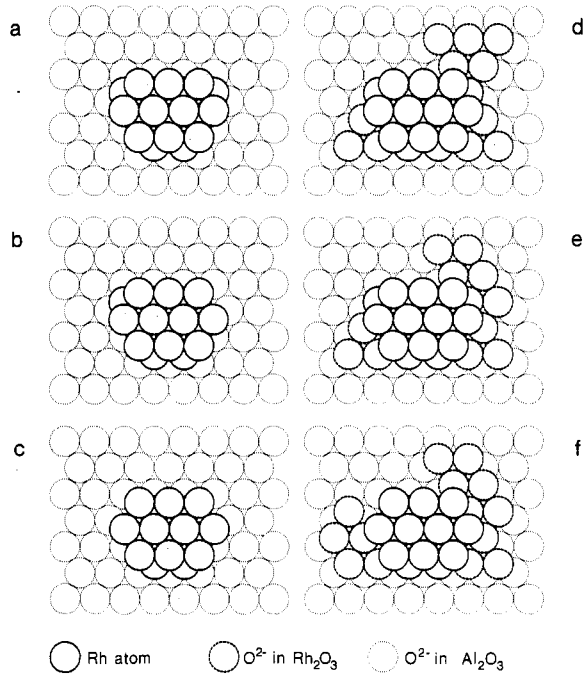

Figure 5. Model of the rhodium metal particles of γ-Al_2O_3 after oxidation at 100 K: (a) bare 19-atom rhodium metal particle; (b) bare 18-atom rhodium metal particle; (c) bare 17-atom rhodium metal particle; (d) 19-atom rhodium metal particle in contact with Rh_2O_3; (e) 18-atom rhodium metal particle in contact with Rh_2O_3; (f) 17-atom rhodium metal particle in contact with Rh_2O_3.

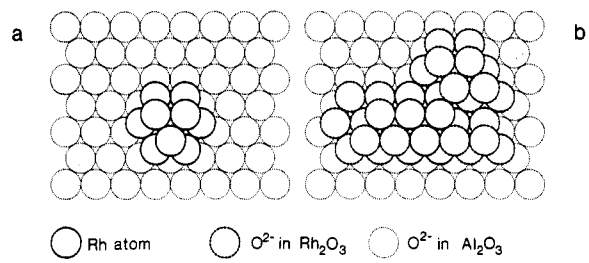

Figure 6. Model of the rhodium metal particles of γ-Al_2O_3 after oxidation at 300 K: (a) bare 10-atom rhodium metal particle; (b) 10-atom rhodium metal particle in contact with Rh_2O_3.

We constructed several models consisting of particles containing approximately 24 ± 3 metal atoms. We found that is was impossible to reproduce the measured Rh^0–O^{2-} coordination number of 2.0 with situations that are principally different from the situation depicted in Figure 4c,d. In all cases, it was essential that rhodium oxide was in contact with the metal particle. In this rhodium–rhodium oxide interface the same kind of Rh^0–O^{2-} distances are present as in the metal–support interface. We therefore assume that Figure 4c,d gives a fairly accurate description of the metal particles in the catalyst after reduction and evacuation. As a consequence, the 26-atom metal particle in Figure 3 will give a good representation of the average metal particle in our Rh/Al_2O_3 sample directly after reduction. When we take into account the inaccuracies in the Rh^{3+}–O^{2-} coordination number, we find that $0.3 < N < 0.9$. From this we calculate that $0.08 < f_{ox} < 0.23$. This indicates that about two to six rhodium atoms were oxidized. In the above calculations we assumed that only three rhodium atoms were oxidized. Clearly, when the inaccuracies are taken into account, this value represents a lower limit. When we assumed that more rhodium metal atoms were oxidized, f_{ox} would be larger than assumed above. Therefore, N_{Rh-Rh} would be larger (7.3 for f_{ox} = 0.23) as well as $N_{Rh-O^{2-}}$ (2.6). This latter coordination number again is too high to account only for oxygen neighbors in the metal–support interface. We could not construct any model of such a metal particle (N_{Rh-Rh} = 7.3 and $N_{Rh-O^{2-}}$ = 2.6) that was only in contact with the Al_2O_3 support and not in contact with rhodium oxide. Thus, we conclude that

after the start of the oxidation process rhodium oxide is in contact with the metal particle.

3. *Rh/Al_2O_3 after Oxygen Admission at 100 K.* After admission of oxygen to the catalyst at 100 K, the EXAFS spectrum changed drastically (see Figure 1). The Rh^0–Rh^0 contribution drastically diminished, and the contribution of the oxidic type of Rh^{n+}–O^{2-} bonds increased in magnitude (cf. Table I). Clearly oxidation has occurred.

We continue to describe the oxidation process as indicated in the foregoing section. Assuming that the rhodium ions in the oxide phase have four to six oxygen neighbors, we find that $0.23 < f_{ox} < 0.35$, indicating that six to nine rhodium atoms have been oxidized. Thus, the remaining metal particles contain 17–20 rhodium atoms. Using the same procedure as described above, we find that successively atoms 5, 1, 9, 4, 14, 15, and 16 will be oxidized (i.e., "removed" from the metal particle). The calculated and averaged Rh^0–Rh^0 coordination number is 4.46, which is higher than the measured value of 4.1. In this situation, atoms 10 and 13 both have a low binding energy. Removing only atom 10 or 13 gives a 19-atom metal particle with a Rh^0–Rh^0 coordination number of 4.15, in very good agreement with the measured value. However, because of their low binding energy, it is more likely that both atoms 10 and 13 are oxidized at the same time. In that situation, the Rh^0–Rh^0 coordination number is 3.85. Again, we assume that reality is an average of two or possibly three situations. In all cases, atoms 5, 1, 9, 4, 14, 15, and 16 are oxidized. In addition, (a) no atoms, (b) one atom (10 or 13), or (c) both atoms 10 and 13 may be oxidized. The average Rh^0–Rh^0 coordination number will be somewhere between 3.85 and 4.46. With the two situations most likely to occur, situations a and c, in a one-to-one ratio, the average Rh^0–Rh^0 coordination number would be equal to 4.1 and would be in excellent agreement with the experimental data.

The calculated Rh^0–O^{2-} coordination numbers (averaged over all 26 rhodium atoms and ions) of the 19, 18, and 17 bare atom metal particles (Figure 5a–c) are 1.04, 0.93, and 0.81 respectively. They are too low compared to the measured value of 1.4. Figure 5d–f gives a representation of a possible arrangement of rhodium oxide around a remaining 19-, 18-, and 17-rhodium metal particle after 7, 8, and 9 atoms have been oxidized. The calculated Rh^0–Rh^0 coordination number (4.15, the average over 4.46, 4.15, and 3.85 for the 19-, 18-, and 17-atom metal particle) agrees very well with the measured value (4.1), and the calculated and measured Rh^0–O^{2-} coordination numbers (1.5 and 1.4, respectively) also agree nicely. Clearly, at least part of the rhodium oxide is in contact with the metal particle. Obviously, the interface between rhodium metal particle and rhodium oxide is rather stable under the experimental conditions.

4. *Rh/Al_2O_3 after Warming up to 300 K under Oxygen.* After oxygen admission at 100 K, the sample was warmed to 300 K under oxygen atmosphere. The resulting spectrum (Figure 1c) was completely different from the two other spectra. The most dominant contribution is now from oxidic Rh^{n+}–O^{2-} bonds and almost no Rh^0–Rh^0 contribution is left (see Table I).

From the measured Rh^{n+}–O^{2-} coordination number, we calculate that $0.60 < f_{ox} < 0.90$. However, because oxidation has progressed that far, we expect that the number of oxygen neighbors in the rhodium oxide phase will be close to 6 and therefore the fraction of oxidized rhodium atoms will be close to 0.6. That means that about 16 atoms will be oxidized and about 10 atoms will remain metallic. Our model calculations indicate that during the oxidation as observed, atoms 17, 19, 20, 23, 24, 25, and 26 will be oxidized as well. The calculated Rh^0–Rh^0 coordination number of the remaining particle, averaged over all 26 rhodium atoms, is 1.85, is in good agreement with the measured value of 1.9. (The Rh^0–Rh^0 coordination number averaged only over the 10 atoms in the remaining metallic kernel of the particle, the *corrected* coordination number, is 4.8.) We once more found it imperative that at least part of the rhodium oxide formed is in contact with the metal particle, and compared to the situation in the preceding paragraph, the rhodium metal-to-rhodium oxide interface has even increased in magnitude. In Figure 6a, a bare 10-atom metallic kernel is shown. For this metal particle, if not covered with rhodium oxide, the Rh^0–O^{2-} coordination number is 0.81, which is about a factor of 2 lower than the measured value (1.7). Figure 6b represents a plausible arrangement of rhodium oxide around the 10-atom metallic kernel.

5. *General Remarks.* In the discussion above, we used the Rh^0–Rh^0 coordination numbers determined with EXAFS to estimate the size of the metal particles and the Rh^{n+}–O^{2-} coordination numbers to estimate the amount of oxidized rhodium. The Rh^0–O^{2-} coordination numbers were used to estimate the extent of the interface between metal and oxide. The accuracy of the latter coordination number, however, is lower than that of the others. The reason for this is shortly as follows. We used a Rh^0–Rh^0 absorber–scatterer pair (R = 2.687, the Rh–Rh distance in bulk rhodium) to extract $F(k)$ and $\phi(k)$ and used these to calculate Rh^0–Rh^0 EXAFS spectra with R = 2.63–2.645 Å, very close to the reference. The Rh^{n+}–O^{2-} EXAFS functions (with R = 2.03–2.055 Å) were calculated using the absorber–scatterer pair Rh^{3+}–O^{2-} (R = 2.05 Å). The coordination distances in calculated EXAFS function and reference compound differ only slightly, and therefore, also this calculation is reliable. However, to use the same absorber–scatterer pair to calculate Rh^0–O^{2-} EXAFS spectra with R = 2.7 Å is not correct. Mainly because of the longer distance, the calculated coordination number underestimates the real coordination numbers. The extent of underestimation may be as much as 20%.[12,31] However, this does not affect our main conclusion that during oxidation a rhodium–rhodium oxide interface is formed. Since the real Rh^0–O^{2-} coordination numbers will be *higher* than the values reported in Table I, the metal–oxide interfaces will even be larger and the coverage by rhodium oxide on the metal particles will be more complete.

In the above discussion it was assumed that energetic considerations played the key role during the oxidation process. However, as oxidation proceeds, the metal particles become covered with rhodium oxide. As a consequence, diffusion will sooner or later become the rate-limiting step in the oxidation process. In the situation described above, we assumed that rhodium atoms with the lowest binding energy will be oxidized. The binding energy calculations indicate that metal atoms that become oxidized have a (relative) binding energy less than 4.1 (or less than five rhodium nearest neighbors). In the metal particles in Figures 3–5, all rhodium atoms which have this low binding energy, and which are to be oxidized in the next step, are exposed to the gas atmosphere, and therefore, a kinetic limitation of the oxidation process is most unlikely. In Figure 6, a 10-atom metal particle is shown. In this metal particle, six rhodium atoms have a binding energy lower than 4.1 (and less than five rhodium neighbors). Therefore, these are candidates to be oxidized in the next stage. They are, however, (partly) covered with rhodium oxide and oxidation may therefore be hampered by diffusion. The three top rhodium atoms still have a binding energy of 4.9, far above the limit (4.1) we used in order to establish whether an atom will be oxidized. Thus, the situation in Figure 6b may represent a stable situation in which oxidation will proceed only after the temperature is elevated. Obviously, up to temperatures of about 300 K, oxidation is not limited by diffusion under the experimental conditions: the oxidic skin is too small to screen the metallic kernel from the surrounding gas phase.

Even after oxidation (passivation) at 300 K, some clean metal surface is still exposed (see Figure 6b); the Rh^0–O^{2-} coordination number was too low to account for complete coverage. The binding energy of the three rhodium atoms on top is 4.9 and they are therefore rather stable. This may very well explain why passivated metal particles are very easily reduced: the metallic kernel adsorbs and dissociates hydrogen even at low temperature and, because of the dissociated (activated) hydrogen, reduction of the neighboring oxide phase is very fast and can proceed at temperatures far below the reduction temperature of the bulk oxide.

(31) Stern, E. A.; Bunker, B. A.; Heald, S. M. *Phys. Rev. B* **1980**, *21*, 5521.

In most cases, during oxidation, the rhodium atom that was to be oxidized in a next stage of oxidation had a binding energy in the range of 4.0. In some cases, removing one rhodium atom resulted in a severe decrease in binding energy of one of its direct nearest rhodium neighbors. In those cases, we assumed that this weakly bound rhodium atom would be oxidized immediately. We never encountered situations in which more than two atoms would be oxidized at the same time. Therefore, we conclude that oxidation has to be a rather smooth and straightforward process.

The rhodium metal particles and rhodium oxide phase have been grown epitaxially on the Al_2O_3[111] crystal face, which is not unlikely for small metal particles or for oxide particles. It has been shown that rhodium oxide grows epitaxially on rhodium [111]. According to Castner and Somorjai[32] Rh_2O_3[0001] fits on Rh[111] when the rhodium oxide unit cell expands by about 5%. The strain induced by this mismatch has only a very small influence on the cohesive energy calculated by using the Lennard-Jones potentials. Rh_2O_3 has the same corundum structure as Al_2O_3. Epitaxial growth of rhodium oxide on the alumina support is also not unlikely. Altogether, the assumptions made in the model described above, epitaxial growth of rhodium particles on the alumina support and epitaxial growth of rhodium oxide on both rhodium metal particles and alumina support, seem justified.

We used only the rhodium atoms in the metal particle in calculating the Lennard-Jones binding energies of the rhodium atoms; the influence of neighboring oxygen ions has been neglected. The additional contribution of oxygen neighbors is expected to be small and not to influence the results significantly. In ref 24 we published results obtained from ASED-MO calculations on a model Al_2O_3 supported rhodium catalyst. We studied the binding of rhodium metal particles on Al_2O_3 surfaces using the ASED-MO method described by Anderson et al.[33] From that study we could conclude that the interaction between zerovalent rhodium atoms in the metal–support interface was lower than the interaction between two neighboring rhodium metal atoms by more than a factor of 2. The Rh–O binding energy ranged from 7 to 21 kcal mol^{-1}, and the Rh–Rh binding energy was approximately 40–80 kcal mol^{-1}, depending on the size of the metal particle. In that study we also found that in case the rhodium metal particles rested in a hydroxylated Al_2O_3 surface, each rhodium atom in the metal–support interface had three neighboring surface $-OH^-$ groups. The accompanying Rh–O coordination distance was approximately 2.6 Å, which is in good agreement with our previous EXAFS results. When the rhodium metal particles in ref 24 rested on a fully dehydroxylated surface, the rhodium atoms in the metal–support interface had bare O^{2-} neighbors at approximately 2.1 Å. During the EXAFS measurements, however, this situation is unlikely to occur. The H_2O partial pressure in the EXAFS cell under the vacuum conditions this study was high enough to maintain a fully hydroxylated Al_2O_3 surface and a fully hydroxylated rhodium oxide surface. Therefore, we believe that in our previous EXAFS studies and in the present study we dealt with metal to surface $-OH^-$ contributions rather than with metal to surface O^{2-} contributions.

In the discussion above we described the oxidation of a 26-atom rhodium metal particle. We applied the same procedure to metal particles ranging from 22 to 30 atoms per particle in order to find out whether the observed trends also hold for these particles. In all cases we found no major differences, and the results presented above and the conclusions to be presented below are representative for the cases we have studied.

Conclusions

Using Rh^0–Rh^0, Rh^0–O^{2-}, and Rh^{n+}–O^{2-} coordination numbers determined with EXAFS, a model has been derived to describe the oxidation of small rhodium metal particles supported on Al_2O_3. After reduction, the metal particles are about 15 Å in diameter and contain about 26 rhodium atoms; after evacuation, the particles are partly oxidized, either by water formed during evacuation or by leaking in of oxygen, and the metal particles contain about 22–24 atoms. After oxygen admission at 100 K, oxidation proceedes and the metal particles contain about 17–19 rhodium atoms. After the catalyst is warmed under oxygen to 300 K, the remaining metal particles contain only about 10 rhodium atoms. The Rh^0–O^{2-} coordination numbers indicate that in all cases the rhodium oxide formed is in contact with the metal particles. Thus, the remaining metallic kernel is partly covered with rhodium oxide. In these new metal-to-metal oxide interfaces, the distance between interfacial zerovalent rhodium atoms and oxygen ions is about 2.7 Å, in accordance with literature data. We therefore conclude that, under the experimental conditions, the rhodium–rhodium oxide interface is more or less stable. Our main conclusion is that during oxidation of small metal particles new metal–support interfaces are formed that can be detected with EXAFS.

Acknowledgment. This study was supported by the Netherlands Foundation for Chemical Research (SON) with financial aid form from the Netherlands Organization for the Advancement of Pure Research (ZWO). We acknowledge the skillful assistance of the Daresbury SRS staff. Finally, during the EXAFS measurements, the invaluable assistance of several colleagues from the Eindhoven University (F. W. H. Kampers, F. B. M van Zon, and J. van Grondelle) cannot remain unmentioned.

Registry No. Rh, 7440-16-6; O_2, 7782-44-7.

(32) Castner, D. G.; Somorjai, G. A. *Appl. Surf. Sci.* **1980**, *6*, 29.
(33) Anderson, A. B.; Ravimohan, Ch.; Mehandru, S. P. *Surf. Sci.* **1987**, *183*, 438.